# Absorption of a weak probe in singly charged n-doped quantum dots in the Voigt geometry

**F. Carreño**

Facultad de Óptica y Optometría, Universidad Complutense de Madrid, C/ Arcos de Jalón 118, 28037 Madrid, Spain

E-mail: ferpo@fis.ucm.es

**M.A. Antón**

Facultad de Óptica y Optometría, Universidad Complutense de Madrid, C/ Arcos de Jalón 118, 28037 Madrid, Spain

E-mail: antonm@fis.ucm.es

**Abstract.** We analyze the absorption of a weak probe field in singly charged $n$-doped quantum dots in the presence of an external magnetic field in the Voigt geometry. The dots are modeled as double lambda systems. A laser field pumps two of the four active transitions while a probe field is applied along the two undriven transitions. It is shown that for both on resonance and out of resonance driving gain (without inversion) is obtained at two sidebands of the dressed QDs. We found that the peak value of gain can be maximized by a proper selection of both the external magnetic field and the Rabi frequency of the pump field for out of resonance driving. We also show that the coherent driving in combination with above-band excitation allows one to turn the absorption peaks into gain (with inversion) in the whole spectral range.

PACS numbers: 32.80.Qk, 42.55.f, 42.50.Hz

*Keywords*: Atomic coherence effects, coherent population trapping, gain without inversion Submitted to: *Laser Phys.*

## 1. Introduction

The absorption of a weak signal field by a strongly driven two-level system was adressed in the early 1970s in the pioneering work due to Mollow[1]. There it was predicted that negative values of absorption (amplification or gain) could be obtained at certain frequencies differing from the frequency of the strong field. This would happen when the on resonance driving-field intensity saturates the transition. This prediction was later experimentally confirmed [2, 3]. It was also shown that when the strong field is set out of resonance one of the sidebands exhibits a strong absorption of the weak probe while the other presents gain [3]. This phenomenon has been demonstrated in a variety of physical systems ranging from different species of atoms[4], quantum wells[5], and superconducting qubits[6].

On the other hand quantum dots (QDs) are a salient solid-state platform for the study of ligth-matter interactions. They are small semiconductor islands of nanometre size that, in spite of being formed by hundreds of thousands of atoms, have an electronic structure consisting of discrete energy levels similar to those of an atom. As such they are often referred to as artificial atoms. Much of the research into these systems has focused either on better understanding the confined energy states of electron and holes within them, and also on how to exploit their quantum nature for practical applications. Those applications range from the coherent manipulation of exciton wave functions[7], optical pumping[8, 9, 10, 11, 12], resonance fluorescence [13, 14, 15, 16, 17, 18, 19, 20, 21, 22, 23, 24, 25, 26, 27, 28, 29, 30, 31], single photon generation [26, 32], rotations of the spin vector[33, 34, 35, 36, 37], quadrature squeezing and antibunching[38], coherent population trapping[39, 40, 41, 42, 43, 44], all-optical switching[45], to the entanglement of distant QDs[46], and they have helped to unlock their potential.

Neutral excitons in QDs have been shown to exhibit spectral features in the Mollow absorption spectrum like the ones found in atomic media [47, 48]. In particular it was shown that gain without population inversion could be obtained when both the pump and probe fields drive the same excitonic transition. A similar result was obtained in the case of a singly charged QD and in the absence of an external magnetic field[49]: there a two-level model was used to account for the experimental findings. However, the spectral structure of charged QDs can be modified by the application of an external magnetic field either along the growth direction (the Faraday geometry) or perpendicular to the growth direction (Voigt geometry). This change arises from the lift of degeneracy of the ground and excited levels due (Zeeman splitting) which results in the so-called double $\Lambda$ system. In what follows we consider singly charged QDs in the Voigt geometry pumped by a strong laser field which drives two of the four allowed transitions and we investigate the absorption of a weak signal which "reads" the state of the system as prepared by the driving field. We show that the probe may experience vanishing absorption as a consequence of CPT when the two-photon resonance condition is met, while at other sidebands the probe field may be amplified without population inversion in the bare

basis. We also show that when the strong field is out of resonance, the level of gain can be maximized by a proper selection of the external magnetic field and the Rabi frequency of the driving field. We also consider the combination of nearly resonant and above-band excitation to control the absorption of the probe field. It is shown that in the strong incoherent pumping regime absorption turn into gain with inversion in the whole spectral range.

The paper is organized as follows: Section 2 establishes the model, i.e. the Hamiltonian of the system and the time-evolution equations of the atomic operators assuming the rotating wave approximation. Section 3 present the results of numerical simulations together with a physical explanation of the different effects found. Finally, Section 4 summarizes the main conclusions.

## 2. Theoretical model

We consider InAs/GaAs self-assembled QDs with growth direction along the $Z$-axis embedded in a $n$-type charge-tunable heterostructure to which a voltage is applied [50, 51]. The application of an external magnetic field along the axis perpendicular to the $Z$-axis, in the so-called Voigt geometry, lifts the degeneracy of hole/electron levels according to $E_{Zm}^{h(e)} = \frac{1}{2}\mu_B g^{h(e)} B_x$, where $E_{Zm}^{h(e)}$ stands for the Zeeman energy shift relative to $B_x = 0$ T, $B_x$ being the external magnetic field, and $\mu_B$ is the Bohr magneton. Quantity $g^{h(e)}$ is the Landé factor of carrier $h(e)$. Each ground state ($|1\rangle$ and $|2\rangle$) is linked to the two exciton states ($|3\rangle$, and $|4\rangle$) via linearly and orthogonally polarized transitions as depicted in Fig. 1.

The Hamiltonian that governs the dynamics of the QD can be expressed in the rotating-wave approximation as

$$H = H_A + H_{Int} \ . \tag{1}$$

The free Hamiltonian $H_A$ of the system reads as

$$H_A = \hbar \sum_{j=1}^{4} \omega_j \sigma_{jj} \ , \tag{2}$$

where $\hbar\omega_j$ is the energy of the j-th level and $\sigma_{ij}$ are the Pauli operators.
The interaction Hamiltonian $H_{Int}$ is written as

$$H_{Int} = \ -\hbar \left( \Omega_{31} e^{-i\omega_L t} \sigma_{31} + \Omega_{42} e^{-i\omega_L t} \sigma_{42} + H.c. \right) \ , \tag{3}$$

accounts for the interaction of the QD with the optical field of angular frequency $\omega_L$ which drives transitions $|1\rangle \leftrightarrow |3\rangle$ and $|2\rangle \leftrightarrow |4\rangle$, while transition transitions $|1\rangle \leftrightarrow |4\rangle$ and $|2\rangle \leftrightarrow |3\rangle$ remain undriven. The Rabi frequencies are given by $\Omega_{31} = \vec{\mu}_{13} \cdot \vec{E}_0 \hbar/2$ and $\Omega_{42} = \vec{\mu}_{24} \cdot \vec{E}_0 \hbar/2$, $\vec{E}_0$ being the slowly varying amplitude of the optical field.

We make use of the unitary transformation $U(t) = e^{-i\omega_L(\sigma_{33}+\sigma_{44})t}$, thus the new Hamiltonian in the rotating frame reduces to

$$H = \ +\hbar\omega_{21}\sigma_{22} + \hbar\delta\sigma_{33} + \hbar(\delta - \omega_{34})\sigma_{44} - \hbar \left( \Omega_{31}\sigma_{31} + \Omega_{42}\sigma_{42} + H.c. \right) \tag{4}$$

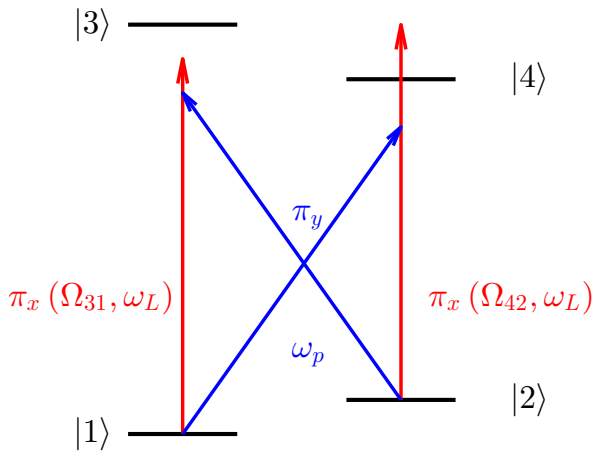


**Figure 1.** Four level system including the relevant transitions when the external magnetic field is applied perpendicular to the growth direcion. Transitions $|1\rangle \leftrightarrow |3\rangle$ and $|2\rangle \leftrightarrow |4\rangle$ are driven by a $\pi_x$ polarized laser field ($\Omega_{31} = \Omega_{42} = \Omega$, pump field) with angular frequency $\omega_L$, while transitions $|1\rangle \leftrightarrow |4\rangle$ and $|2\rangle \leftrightarrow |3\rangle$ are "read" by a $\pi_y$ probe field of angular frequency $\omega_p$.

where $\delta \equiv \omega_{31} - \omega_L$ stands for the optical detuning along transition $|1\rangle \leftrightarrow |3\rangle$, and $\omega_{kl} = \omega_k - \omega_l$.

The time evolution of the density matrix reads as

$$\frac{\partial}{\partial t}\rho = -\frac{i}{\hbar}\left[H,\rho\right] + \mathcal{L}\rho\,, \tag{5}$$

$\mathcal{L}\rho$ being the Liouvillian of the system which reads $\mathcal{L}\rho = \sum_{j=1,2;k=3,4} L(\sqrt{\Gamma_{kj}}\sigma_{jk}) + \sum_{j=1,2;k=3,4} L(\sqrt{\Lambda_i}\sigma_{kj}) + L(\sqrt{\Gamma_{12}}\sigma_{12}) + L(\sqrt{\Gamma_{21}}\sigma_{21}) + \sum_{i=1}^{2} L(\sqrt{\gamma_{ii}}\sigma_{ii})$. The terms involving $\Gamma_{kj}$ arise from Linblad operators which account for the spontaneous photons produced along transitions $|k\rangle \leftrightarrow |j\rangle$, the terms proportional to $\gamma_{ii}$ $(i = 1, 2)$ accounts for pure dephasing, whereas the terms proportional to $\Gamma_{21}$, and $\Gamma_{12}$ arise from an incoherent relaxation process which couples states $|1\rangle \leftrightarrow |2\rangle$ bidirectionally. They arise from exchange interaction with the Fermi sea of electrons in the back contact giving rise to spin-flip cotunneling. Finally the terms involving $\Lambda_i$ account for above-band incoherent pumping. The action of a Linblad operator is defined as: $L(C) = C\rho C^\dagger - \frac{1}{2}(\rho C^\dagger C + C^\dagger C\rho)$.

We project both sides of Eq. (5) onto the set of states $|j\rangle\,, (j = 1, 4)$, and derive the coupled equations of motion for the density matrix elements. It is convenient to define the following vector:
$U(t) = [\rho_{22}(t), \rho_{33}(t), \rho_{44}(t), \rho_{21}(t), \rho_{12}(t), \rho_{31}(t), \rho_{13}(t), \rho_{41}(t), \rho_{14}(t), \rho_{32}(t), \rho_{23}(t), \rho_{42}(t), \rho_{24}(t), \rho_{43}(t), \rho_{34}(t)]^T$, where superscript $T$ stands for transpose, in such a way that the equa-

tions of motion of the density matrix elements is reduced to a simple expression

$$\frac{d}{d\,t}U(t) = MU(t) + B\,, \tag{6}$$

with $M$ being an $(8\times 8)$ matrix, and $B$ a column vector whose coefficients can be easily determined. Steady-state values for populations and coherences are derived through $U(\infty) = M^{-1}(-B)$.

We are interested in determining the absorption spectrum of a weak probe field which is applied along the diagonal transitions. We assume that the Rabi frequency along the probed transitions is much lower than the Rabi frequencies along the vertical transitions (pump fields), in such a way that the probe field does not alter the population redistribution produced by the strong driving fields. In the steady-state regime, the a absorption spectrum is determined through the conmutator of the atomic polarization operator [1, 52], and can be expressed as

$$A(\omega) \propto Re\left\{\lim_{t\to\infty}\int_0^\infty \langle\left[D^-\left(t'+t\right), D^\dagger\left(t\right)\right]\rangle e^{-i\omega t'}dt'\right\}\,, \tag{7}$$

where $Re\left[\,\right]$ denotes the real part of the magnitude enclosed in square brackets, and $D^-\left(t\right)$ is the negative frequency part of the atomic polarization operator which reads

$$D^-(t) = \mu_{14}\sigma_{14}(t) + \mu_{23}\sigma_{23}(t)\,, \tag{8}$$

and $\mu_{14} = \hat{e}_p\cdot\vec{\mu}_{14}$, and $\mu_{23} = \hat{e}_p\cdot\vec{\mu}_{23}$, $\hat{e}_p$ being the unit polarization vector of the probe field.

In writing Eq. (7), we abbreviate $\omega_p - \omega_L$ by $\omega$, but we should interpret $\omega$ as the frequency of the probe field measured relative to the laser frequency $\omega_L$ since we will assume that the QD is driven by $\pi_x$ polarized laser field. The calculation of $A(\omega)$ requires to evaluate two-time correlation functions, which can be performed by means of the quantum-regression theorem [53, 52].

## 3. Numerical results

We consider the four levels of the electron-trion system in the Voigt geometry. The system is driven by a $\pi_x$ polarized laser field detuned by $\delta$ from the $|3\rangle \leftrightarrow |1\rangle$ transition. The excited level relaxes to both ground states with decay rates $\Gamma_{31}$ and $\Gamma_{32}$. The same laser also drives the transition $|4\rangle \leftrightarrow |2\rangle$ in an off resonant way which in turn results in a small pumping of population in the opposite direction with decay rates $\Gamma_{41}$ and $\Gamma_{42}$. In what follows we assume that $\Gamma_{41} = \Gamma_{42} = \Gamma_{32} = \Gamma_{31} \equiv \Gamma_0 = 1.2\,\mu$eV, and we consider the $g$ factors $g^e = -0.46$ and $g^h = -0.29$, as in Ref. [10]. Dephasing rates $\gamma_{11} = \gamma_{22} = 0.08\Gamma_0$, and cotunneling rates $\Gamma_{12} = \Gamma_{21} = 0.004\Gamma_0$ are taken from Ref. [14]. We also assume that transition dipole moments are equal, i.e., $\vec{\mu}_{13} = \vec{\mu}_{24}$, which in turn results in $\Omega_{13} = \Omega_{24} \equiv \Omega$. We also consider the possibility of incoherent pumping of the four allowed transitions with a pump rate $\Lambda_i$ as in Ref. [31].

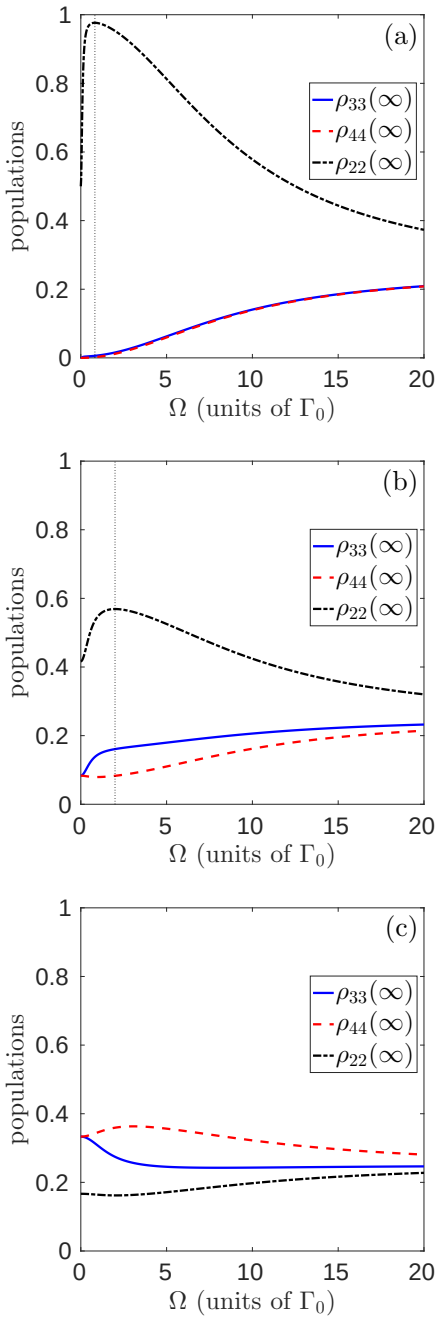


**Figure 2.** Steady-state population of the states versus the Rabi frequency of the driving field $\Omega$: $|3\rangle$ (solid curve), $|4\rangle$ (dashed curve) and $|2\rangle$ (dashed-dotted curve). Numerical values used are: $B_{ext} = 1$ T, $\Gamma_0 = 1.2\mu$eV, $\gamma_{11} = \gamma_{22} = 0.08\Gamma_0$ , $\Gamma_{12} = \Gamma_{21} = 0.004\Gamma_0$ , and $\delta = 0$. (a) $\Lambda_i = 0$, (b) $\Lambda_i = 0.2\Gamma_0$, and (c) $\Lambda_i = 2\Gamma_0$.

### *3.1. Steady state populations*

In the context of performing state operations over the qubit formed by the two lower levels, and as a result of the non-deterministic charging of the QD, optical pumping is required to initialize the state of the QD. This topic was analyzed in detail in Ref. [10],

where it was shown that in the case of applying a strong magnetic field (in the order of 4 T), the four-level system could be approximately described as a $\Lambda$-type atomic scheme. Here we are interested in the regime of low to moderate magnetic fields, therefore population redistribution among the four levels is essential. To this end we start by considering the effect of resonant excitation of the transition $|1\rangle \leftrightarrow |3\rangle$ while we set $\Lambda_i = 0$. The results obtained in the case of considering an external magnetic field of $B_{ext} = 1$ T are shown in Fig. 2(a) for the case with $\delta = 0$: there we can appreciate that the two upper levels almost share the same level of population while level $|2\rangle$ is highly populated at a particular Rabi frequency ($\Omega_{opt}$) where optical pumping is relatively high. Driving the system far from $\Omega_{opt}$ results in an inefficient optical pumping which manifests in the obtention of moderate to high values of populations in the upper states. This effect originates from the out-of-resonance driving field $\Omega_{42}$ which repumps population back from level $|2\rangle$. Here we will see that this repumping mechanism, which is deleterious for the purpose of efficient spin pumping, allows one to obtain gain at certain sidebands. The existence of an optimum Rabi frequency which maximizes the transfer of population to level $|2\rangle$ also holds in the case of driving the system out of resonance ($\delta \neq 0$). Results of numerical simulations show that (i) the value of $\Omega_{opt}$ depends on the sign of $\delta$, and (ii) such those values for $\Omega_{opt}$ are always greater than the ones obtained for the case with resonant excitation.

Now we consider the effect of incoherent pumping on the redistribution of populations. An example of such redistribution is shown in Fig. 2(b) which was produced for the same data as in panel 2(a) but $\Lambda_i = 0.2\Gamma_0$. Here we can devise that optical pumping is completely frustrated and that population of states $|3\rangle$ and $|4\rangle$ grow apart as the Rabi frequency is changed. Results of numerical simulations show that these results hold when (i) the coherent field is non-resonant ($\delta \neq 0$), and (ii) the external magnetic field is increased.

Up to now, we have kept fixed the incoherent pumping rate. In the case of considering a strong incoherent pumping, let's say $\Lambda_i = 2\Gamma_0$, steady-state population of upper levels surpasses that of level $|2\rangle$ for the whole range of $\Omega$ as shown in Fig. 2(c). This behaviour is expected since population is pumped from lower to upper levels at a rate greater than the spontaneous decay rates.

### *3.2. Probe absorption under coherent driving*

Now we focus on the absorption spectrum of a weak probe along the undriven transitions in the absence of incoherent pumping. The results obtained for on resonant driving ($\delta = 0$) are shown in Fig. 3(a): the dashed curve is produced using the value of $\Omega_{opt} = 0.82\Gamma_0$ which was numerically determined from Fig. 2(a). Here we recover the dip in the absorption profile associated to a non-perfect CPT which is obtained for a value of $\omega_p$ such that the two-photon resonance condition is met. The non-null value at the dip of the spectrum originates from the effect of dephasing and co-tunnelling [39]. When the Rabi frequency of the pump field is increased (solid curve) the level

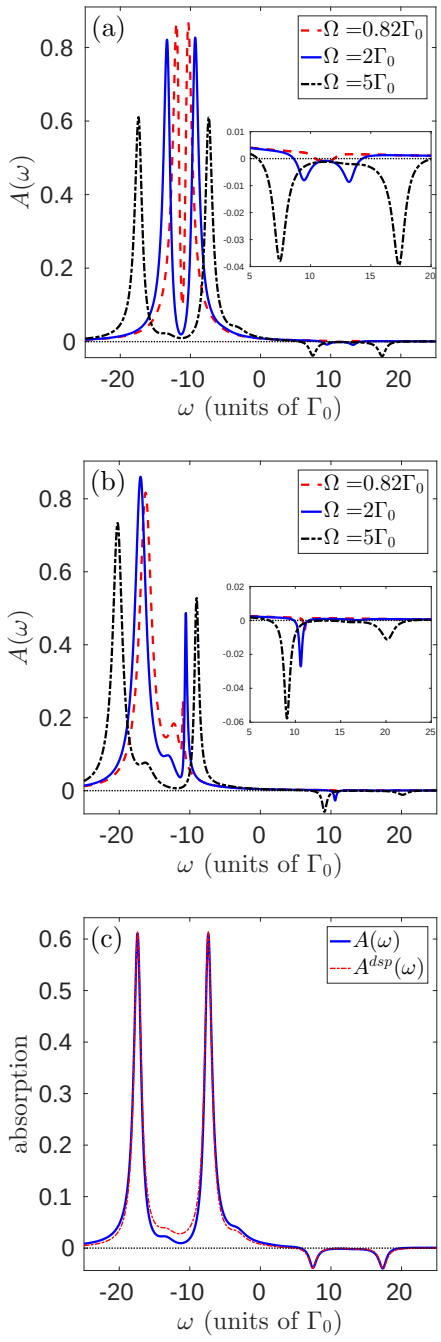


**Figure 3.** Absorption spectrum of a weak probe field along the diagonal channels $[A(\omega)]$ when the system is driven on resonance along the transition $|1\rangle \leftrightarrow |3\rangle$ in the absence of incoherent pumping ($\Lambda_i = 0$) for different Rabi frequencies of the pump field along the vertical transitions: $\Omega = 0.82\Gamma_0$ (dashed curve), $\Omega = 2\Gamma_0$ (solid curve), and $\Omega = 5\Gamma_0$ (dashed-dotted curve). The horizontal dotted line is an eye guide to indicate the null level of absorption. (a) $\delta = 0$, and (b) $\delta = -5\Gamma_0$. (c) Comparison of the absorption computed in the bare basis (solid curve) and the dressed basis (dashed-dotted curve) for the case with $\Omega = 5\Gamma_0$, and $\delta = 0$.

of absorption at the dip is further reduced and there appear two small blue detuned gain peaks. This effect is further enhanced for the largest value of the Rabi frequency (dashed-dotted curve) where the level of gain has increased an order of magnitude with regard to the solid curve. It is worth noting that in view of Fig. 2, the gain is obtained without population inversion in the bare basis.

As for the case in which the system is driven out of resonance, we show the results for the absorption of the weak probe in panel 3(b) for the same Rabi frequencies previously considered and $\delta = -5\Gamma_0$. Here we want to highlight that one of the absorption peaks and one of the gain peaks become subnatural. The most striking feature relies on the fact that the level of gain at the blue sideband with subnatural linewidth is greater than the level obtained for on resonant excitation. The narrowness of the absorption and gain peaks is reminiscent of the subnatural Raman photons appearing in the resonance fluorescence spectrum experimentally studied in Ref. [17]. Those photons still exhibit a subnatural linewidth for a wide range of values of the Rabi frequency of the pump field[30].

The spectral features depicted in Fig. 3(a)-(b) can be explained by moving to the dressed-state picture (DSP). It can be shown that the eigenvalues of the quantum system plus the coherent part of the Hamiltonian are provided by finding the roots of the polynomial

$$+\lambda^4 + b_1\lambda^3 + b_2\lambda^2 + b_3\lambda + b_4 = 0\,, \tag{9}$$

with $b_1 = -(\omega_{21} - \omega_{34} + 2\delta)$, $b_2 = \omega_{21}\delta + (\omega_{21} + \delta)(\delta - \omega_{34}) - 2\Omega^2$, $b_3 = \Omega^2\delta + \Omega^2(\omega_{21} - \omega_{34} + \delta) - \omega_{21}\delta(\delta - \omega_{34})$, and $b_4 = \Omega^2(\Omega^2 - \omega_{21}(\delta - \omega_{34}))$. The roots are labeled as $\lambda_j$ $(j = \alpha, \beta, \gamma, \delta)$ and are sorted in ascending order, i.e., $\lambda_\alpha < \lambda_\beta < \lambda_\gamma < \lambda_\delta$. The corresponding eigenstates are

$$\begin{aligned}
|\alpha\rangle &= a_{2\alpha}|2\rangle + a_{4\alpha}|4\rangle\,,\\
|\beta\rangle &= a_{1\beta}|1\rangle + a_{3\beta}|3\rangle\,,\\
|\gamma\rangle &= a_{1\gamma}|1\rangle + a_{3\gamma}|3\rangle\,,\\
|\delta\rangle &= a_{2\delta}|2\rangle + a_{4\delta}|4\rangle\,,
\end{aligned} \tag{10}$$

where the coefficients are given by $a_{2\alpha} = +\frac{\Omega}{\sqrt{\Omega^2+(\omega_{21}-\lambda_\alpha)^2}}$, $a_{4\alpha} = +\frac{\omega_{21}-\lambda_\alpha}{\sqrt{\Omega^2+(\omega_{21}-\lambda_\alpha)^2}}$, $a_{2\delta} = -\frac{\omega_{21}-\lambda_\alpha}{\sqrt{\Omega^2+(\omega_{21}-\lambda_\alpha)^2}}$, $a_{4\delta} = +\frac{\Omega}{\sqrt{\Omega^2+(\omega_{21}-\lambda_\alpha)^2}}$, $a_{1\beta} = +\frac{\Omega}{\sqrt{\Omega^2+\lambda_\beta^2}}$, $a_{3\beta} = -\frac{\lambda_\beta}{\sqrt{\Omega^2+\lambda_\beta^2}}$, $a_{1\gamma} = +\frac{\lambda_\beta}{\sqrt{\Omega^2+\lambda_\beta^2}}$, $a_{3\gamma} = +\frac{\Omega}{\sqrt{\Omega^2+\lambda_\beta^2}}$.

We can shed light to the features found in the spectra when considering the so-called secular approximation which consists of obtaining equations of motion of populations and coherences while ignoring the coupling between them (the details are provided in Appendix A). Under such condition, the absorption spectrum of the weak probe along the $y$ polarized channels ($A^{dsp}(\omega)$) can be split as a superposition of up to eight Lorentzians whose spectral positions are given by $\Omega_{jk} = \lambda_j - \lambda_k\,(j, k = \alpha, \beta, \gamma, \delta)$ as indicated in Eq. (A.4).

The validity of the secular approximation can be checked by comparing the spectrum obtained using such procedure $\left[A^{dsp}(\omega)\right]$ with the one determined in the bare basis $[A(\omega)]$. Such closeness of the absorption spectra is shown in panel 3(c) for the largest Rabi frequency ($\Omega = 5\Gamma_0$) and the on resonant pumping case ($\delta = 0$). The blue detuned sidebands where gain is obtained originate from transitions $|\delta, N\rangle \leftrightarrow |\gamma, N-1\rangle$, and $|\delta, N\rangle \leftrightarrow |\beta, N-1\rangle$ for the inner and outer sidebands, respectively, and $N$ being the number of photons in the manifold.

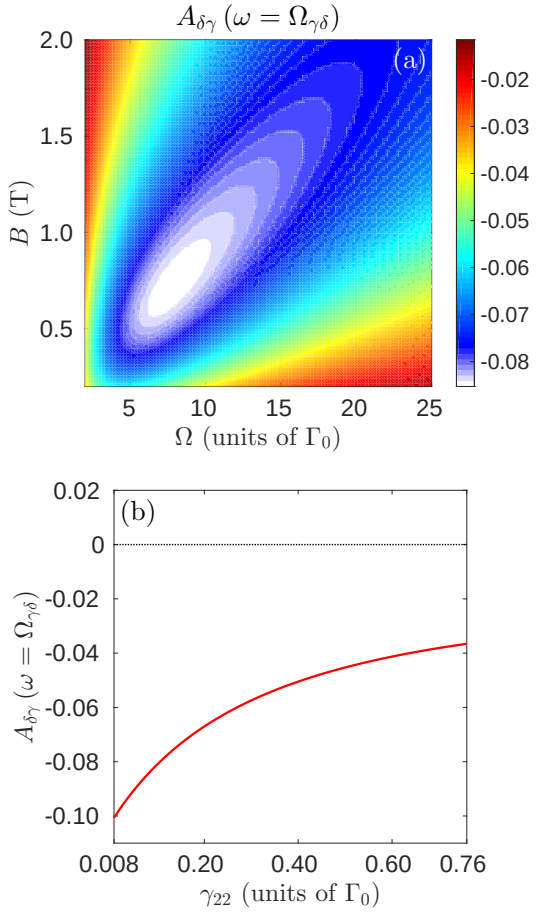


**Figure 4.** (a) Peak value of the gain at the blue detuned inner sideband $[A_{\delta\gamma}\,(\omega = \Omega_{\gamma\delta})]$ versus the Rabi frequency $\Omega$ and the external magnetic field $B$, in the case with $\delta = -10\Gamma_0$, and $\Lambda_i = 0$. (b) Peak value of the gain at the blue detuned sidebands versus the dephasing $\gamma_{22}$ for the case with $\delta = -10\Gamma_0$, $B = 0.72$T, and $\Omega = 7.84\Gamma_0$, and $\Lambda_i = 0$.

Since we have found that the level of gain is higher for non resonant driving ($\delta \neq 0$), now we explore how to optimize the level of gain obtained while considering changes in the Rabi frequency and the external magnetic field. The peak value of the gain at the blue detuned inner sideband can be estimated after a close look to Eq. (A.4) and can be shown to be given by $A_{\delta\gamma}\,(\omega = \Omega_{\gamma\delta}) = (a_{4\delta}a_{1\gamma})^2\,(\langle\sigma_{\gamma\gamma}(\infty)\rangle - \langle\rho_{\delta\delta}(\infty)\rangle)/\Gamma_{\gamma\delta}$. Figure 4(a) presents a contour plot for the level of gain at the blue inner sideband and reveals the existence of a pair of values for the external magnetic field and the Rabi frequency,

$(B_{opt}, \Omega_{opt})$ , which results in the highest gain for a value of $\delta = -10\Gamma_0$. Numerical simulations carried out reveals that the optimum values for the external magnetic field and the Rabi frequency change as the detuning is modified.

QDs are known to be prone to dephasing, thus it is essential to consider whether the obtention of gain is limited by this mechanism. Figure 4(b) presents the change of the peaks values at the blue detuned sidebands as we change the value of $\gamma_{22}$. We have produced this panel assuming that $\gamma_{11} = \gamma_{22}$ while the interval of variation for $\gamma_{22}$ has been taken to be from one tenth to ten times the one used in Fig. 3. In producing this figure we have kept the detuning fixed to $\delta = -10\Gamma_0$, and we selected the optimum values for the external magnetic field and the Rabi frequency determined from panel 4(a), i.e., $B_{opt} = 0.72$ T, and $\Omega_{opt} = 7.84\Gamma_0$. Here we can devise that the level of gain at the blue detuned inner sideband is strongly affected by the level of dephasing. Numerical simulations carried out show that this also happens for the blue detuned outer sideband, in spite of the fact that the level of gain obtained is smaller than for the inner sideband. These two figures are useful to determine the range of parameters to maximize the level of gain.

### *3.3. Effect of incoherent pumping on probe absorption*

Now we move to a situation in which the above-band excitation is present ($\Lambda_i \neq 0$). We have previously seen in Fig. 2(b)-(c) that the incoherent pumping dramatically influences the redistribution of populations among the levels at steady-state. Thus it is expected that this will impact the absorption of the weak probe along the diagonal channels.

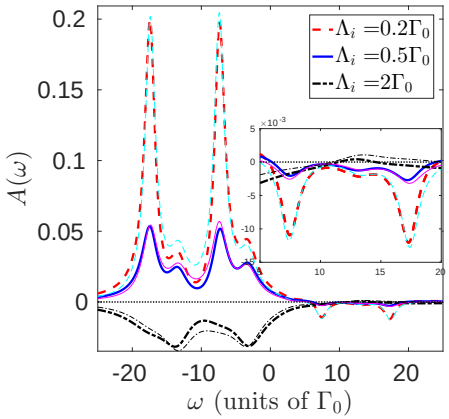


**Figure 5.** Absorption spectrum of a weak probe field along the diagonal channels $[A(\omega)]$ when the system is driven on resonance along the transition $|1\rangle \leftrightarrow |3\rangle$ ($\delta = 0$) with $\Omega = 5\Gamma_0$ for different values of the incoherent pumping: $\Lambda_i = 0.2\Gamma_0$ (thick dashed-dotted curve), $\Lambda_i = 0.5\Gamma_0$ (thick solid curve), and $\Lambda_i = 2\Gamma_0$ (thick dashed-dotted curve). The thin curves account for the probe absorption determined in the DSP through Eq. (A.4).

The absorption of the probe for a fixed resonant coherent driving is shown in Fig.

5. As for the case of the smallest value of $\Lambda_i$ (thick dashed curve) we can see that the main effect is to produce a substantial reduction of the peak values of the absorption obtained for negative values of $\omega$ (compare with dashed-dotted curve in panel 3(a)). In addition, the two gain features produced at positive values of $\omega$ also fade when $\Lambda_i \neq 0$. An increase of the pump rate up to $\Lambda_i = 0.5\Gamma_0$ (thick solid curve) results in a further decrease of the probe absorption over the whole spectral range. Note that in the case $\Lambda_i = \Gamma_0$ (not shown) the probe will be transparent over the entire range of frequencies. Under this particular condition the steady state population fulfill the condition $\rho_{jj}(\infty) = 1/4\,(j = 1, 2, 3, 4)$. This should not come as a surprise, since for this value of $\Lambda_i$ the incoherent pumping cancells the spontaneous emission along the different optical allowed transitions. Moreover, this condition holds independently of the values of the external magnetic field and the Rabi frequency of the coherent field. In the case of the largest incoherent pumping (thick dashed-dotted curve) the two absorption peaks turn into gain over the whole spectral range. However, it should be mentioned that gain here is obtained with inversion along the channels involved in the bare basis. Finally, note that the shape of the absorption spectrum can be reproduced in the DSP under incoherent pumping conditions provided the secular approximation holds (see the closeness of the thin curves to the thick ones in Fig. 5). As for the largest value of $\Lambda_i$, the width of the individual Lorentzians become much greater than $2\Gamma_0$, i.e., a side effect of the above-band excitation is to broaden the transitions between dressed states.

## 4. Conclusions

In this work we present a theoretical description of the spectral properties of a weak probe field acting along the diagonal transitions of singly charged $n$-doped QDs in the Voigt geometry which is driven by a strong optical field along the vertical transitions. The absorption spectrum reveals the obtention of CPT which has been already observed in the laboratory for this kind of QDs. In addition, gain without inversion in the bare basis is produced at specific probe frequencies. Numerical simulations reveal that the level of gain can be maximized when the system is driven out of resonance. The influence of dephasing on the probe absorption is also analyzed showing that this is a limiting factor to obtain gain at certain sidebands. We have also considered the possibility of using a combination of nearly resonant and an above-band excitation to control the absorption of the probe field. It is shown that in the regime of low incoherent pumping its effect is to produce an overall reduction of probe absorption, while in the regime of strong incoherent pumping absorption turn into gain (with inversion) in the whole spectral range. The probe absorption features are fully explained by moving to the DSP in the secular approximation where the absorption spectrum of the weak probe is described as a superposition of Lorentzians whose center, amplitudes, and linewidths account for the different numerical findings. The results obtained open the way for the demonstration of various quantum level-based phenomena such as quantum dot lasers, optical modulators, or logic devices.

## Appendix A. Absorption of a weak probe field in the dressed state basis

The equations of motion for populations and coherences in the secular approximation read

$$
\begin{aligned}
\frac{d\langle\sigma_{\alpha\alpha}(t)\rangle}{dt} &= \hat{\Gamma}_{\alpha\alpha}\langle\sigma_{\alpha\alpha}(t)\rangle + \hat{\Gamma}_{\alpha\beta}\langle\sigma_{\beta\beta}(t)\rangle + \hat{\Gamma}_{\alpha\gamma}\langle\sigma_{\gamma\gamma}(t)\rangle + \hat{\Gamma}^0_{\alpha\alpha}\,,\\
\frac{d\langle\sigma_{\beta\beta}(t)\rangle}{dt} &= \hat{\Gamma}_{\beta\alpha}\langle\sigma_{\alpha\alpha}(t)\rangle + \hat{\Gamma}_{\beta\beta}\langle\sigma_{\beta\beta}(t)\rangle + \hat{\Gamma}_{\beta\gamma}\langle\sigma_{\gamma\gamma}(t)\rangle + \hat{\Gamma}^0_{\beta\beta}\,,\\
\frac{d\langle\sigma_{\gamma\gamma}(t)\rangle}{dt} &= \hat{\Gamma}_{\gamma\alpha}\langle\sigma_{\alpha\alpha}(t)\rangle + \hat{\Gamma}_{\gamma\beta}\langle\sigma_{\beta\beta}(t)\rangle + \hat{\Gamma}_{\gamma\gamma}\langle\sigma_{\gamma\gamma}(t)\rangle + \hat{\Gamma}^0_{\gamma\gamma}\,,\\
\frac{d\langle\sigma_{\beta\alpha}(t)\rangle}{dt} &= -\left(\Gamma_{\beta\alpha} - i\Omega_{\beta\alpha}\right)\langle\sigma_{\beta\alpha}(t)\rangle\,,\\
\frac{d\langle\sigma_{\gamma\alpha}(t)\rangle}{dt} &= -\left(\Gamma_{\gamma\alpha} - i\Omega_{\gamma\alpha}\right)\langle\sigma_{\gamma\alpha}(t)\rangle\,,\\
\frac{d\langle\sigma_{\alpha\delta}(t)\rangle}{dt} &= -\left(\Gamma_{\alpha\delta} - i\Omega_{\alpha\delta}\right)\langle\sigma_{\alpha\delta}(t)\rangle\,,\\
\frac{d\langle\sigma_{\beta\gamma}(t)\rangle}{dt} &= -\left(\Gamma_{\beta\gamma} - i\Omega_{\beta\gamma}\right)\langle\sigma_{\beta\gamma}(t)\rangle\,,\\
\frac{d\langle\sigma_{\beta\delta}(t)\rangle}{dt} &= -\left(\Gamma_{\beta\delta} - i\Omega_{\beta\delta}\right)\langle\sigma_{\beta\delta}(t)\rangle\,,\\
\frac{d\langle\sigma_{\gamma\delta}(t)\rangle}{dt} &= -\left(\Gamma_{\gamma\delta} - i\Omega_{\gamma\delta}\right)\langle\sigma_{\gamma\delta}(t)\rangle\,,
\end{aligned}
\tag{A.1}
$$

where $\Omega_{jk} = \lambda_j - \lambda_k$ ($j \neq k$ and $j,k = \alpha,\beta,\gamma,\delta$) stands for the effective Rabi frequencies in the new basis, and the coefficients appearing in Eq. (A.1) involving populations read

$$
\begin{aligned}
\hat{\Gamma}^0_{\alpha\alpha} =& +\Gamma_{42}a^2_{2\alpha}a^2_{4\delta} + \gamma_{22}a^2_{2\alpha}a^2_{2\delta} + \Lambda_i a^2_{2\delta}a^2_{4\alpha}\,,\\
\hat{\Gamma}_{\alpha\alpha} =& -(\Gamma_{42}+\Gamma_{41})a^2_{4\alpha} - (\Gamma_{21}+\gamma_{22})a^2_{2\alpha} - \gamma_{22}a^2_{2\alpha}\\
&- \gamma_{22}a^2_{2\alpha}a^2_{2\delta} - \Gamma_{42}a^2_{2\alpha}a^2_{4\delta} + \Gamma_{42}a^2_{2\alpha}a^2_{4\alpha} + \gamma_{22}a^4_{2\alpha}\\
&+ \Lambda_i\left(a^2_{2\alpha}a^2_{4\alpha} - a^2_{2\delta}a^2_{4\alpha} - 2a^2_{2\alpha}\right)\,,\\
\hat{\Gamma}_{\alpha\beta} =& \Gamma_{32}a^2_{2\alpha}a^2_{3\beta} + \Gamma_{12}a^2_{1\beta}a^2_{2\alpha} - \Gamma_{42}a^2_{2\alpha}a^2_{4\delta} - \gamma_{22}a^2_{2\alpha}a^2_{2\delta}\\
&+ \Lambda_i\left(a^2_{1\beta}a^2_{4\alpha} - a^2_{2\delta}a^2_{4\alpha}\right)\,,\\
\hat{\Gamma}_{\alpha\gamma} =& \Gamma_{32}a^2_{2\alpha}a^2_{3\gamma} + \Gamma_{12}a^2_{1\gamma}a^2_{2\alpha} - \Gamma_{42}a^2_{2\alpha}a^2_{4\delta} - \gamma_{22}a^2_{2\alpha}a^2_{2\delta}\\
&+ \Lambda_i\left(a^2_{1\gamma}a^2_{4\alpha} - a^2_{2\delta}a^2_{4\alpha}\right)\,,\\
\hat{\Gamma}^0_{\beta\beta} =& +\Gamma_{41}a^2_{1\beta}a^2_{4\delta} + \Gamma_{21}a^2_{1\beta}a^2_{2\delta} + \Lambda_i a^2_{2\delta}a^2_{3\beta}\,,\\
\hat{\Gamma}_{\beta\alpha} =& \Gamma_{41}a^2_{1\beta}a^2_{4\alpha} + \Gamma_{21}a^2_{1\beta}a^2_{2\alpha} - \Gamma_{41}a^2_{1\beta}a^2_{4\delta} - \Gamma_{21}a^2_{1\beta}a^2_{2\delta}\\
&+ \Lambda_i\left(a^2_{2\alpha}a^2_{3\beta} - a^2_{2\delta}a^2_{3\beta}\right)\,,\\
\hat{\Gamma}_{\beta\beta} =& -(\Gamma_{32}+\Gamma_{31})a^2_{3\beta} - (\Gamma_{12}+\gamma_{11})a^2_{1\beta}\\
&- \Gamma_{21}a^2_{1\beta}a^2_{2\delta} - \Gamma_{41}a^2_{1\beta}a^2_{4\delta} + \Gamma_{31}a^2_{1\beta}a^2_{3\beta} + \gamma_{11}a^4_{4\beta}\\
&+ \Lambda_i\left(a^2_{1\beta}a^2_{3\beta} - a^2_{2\delta}a^2_{3\beta} - 2a^2_{1\beta}\right)\,,\\
\hat{\Gamma}_{\beta\gamma} =& \Gamma_{31}a^2_{1\beta}a^2_{3\gamma} + \gamma_{11}a^2_{1\beta}a^2_{1\gamma} - \Gamma_{41}a^2_{1\beta}a^2_{4\delta} - \Gamma_{21}a^2_{1\beta}a^2_{2\delta}
\end{aligned}
$$

$$
\begin{aligned}
&+\Lambda_i\left(a_{1\gamma}^2a_{3\beta}^2-a_{2\delta}^2a_{3\beta}^2\right)\ ,\\
\hat{\Gamma}_{\gamma\gamma}^0 &= +\Gamma_{41}a_{1\gamma}^2a_{4\delta}^2+\Gamma_{21}a_{1\gamma}^2a_{2\delta}^2+\Lambda_ia_{2\delta}^2a_{3\gamma}^2\ ,\\
\hat{\Gamma}_{\gamma\alpha} &= \Gamma_{41}a_{1\gamma}^2a_{4\alpha}^2+\Gamma_{21}a_{1\gamma}^2a_{2\alpha}^2-\Gamma_{41}a_{1\gamma}^2a_{4\delta}^2-\Gamma_{21}a_{1\gamma}^2a_{2\delta}^2\\
&\quad+\Lambda_i\left(a_{2\alpha}^2a_{3\gamma}^2-a_{2\delta}^2a_{3\gamma}^2\right)\ ,\\
\hat{\Gamma}_{\gamma\beta} &= \Gamma_{31}a_{1\gamma}^2a_{3\beta}^2+\gamma_{11}a_{1\beta}^2a_{1\gamma}^2-\Gamma_{41}a_{1\gamma}^2a_{4\delta}^2-\Gamma_{21}a_{1\gamma}^2a_{2\delta}^2\\
&\quad+\Lambda_i\left(a_{1\beta}^2a_{3\gamma}^2-a_{2\delta}^2a_{3\gamma}^2\right)\ ,\\
\hat{\Gamma}_{\gamma\gamma} &= -(\Gamma_{32}+\Gamma_{31})a_{3\gamma}^2-(\Gamma_{12}+\gamma_{11})a_{1\gamma}^2\\
&\quad-\Gamma_{21}a_{1\gamma}^2a_{2\delta}^2-\Gamma_{41}a_{1\gamma}^2a_{4\delta}^2+\Gamma_{31}a_{1\gamma}^2a_{3\gamma}^2+\gamma_{11}a_{1\gamma}^4\\
&\quad+\Lambda_i\left(a_{1\gamma}^2a_{3\gamma}^2-a_{2\delta}^2a_{3\gamma}^2-2a_{1\gamma}^2\right)\ ,
\end{aligned}
\tag{A.2}
$$

whereas the coefficients appearing in Eq. (A.1) involving coherences read

$$
\begin{aligned}
\Gamma_{\beta\alpha} &= \frac{\Gamma_{32}+\Gamma_{31}}{2}a_{3\beta}^2+\frac{\Gamma_{42}+\Gamma_{41}}{2}a_{4\alpha}^2+\frac{\Gamma_{21}+\gamma_{22}}{2}a_{2\alpha}^2+\frac{\Gamma_{12}+\gamma_{11}}{2}a_{1\beta}^2+\Lambda_i\left(a_{1\beta}^2+a_{2\alpha}^2\right)\ ,\\
\Gamma_{\gamma\alpha} &= \frac{\Gamma_{32}+\Gamma_{31}}{2}a_{3\gamma}^2+\frac{\Gamma_{42}+\Gamma_{41}}{2}a_{4\alpha}^2+\frac{\Gamma_{21}+\gamma_{22}}{2}a_{2\alpha}^2+\frac{\Gamma_{12}+\gamma_{11}}{2}a_{1\gamma}^2+\Lambda_i\left(a_{1\gamma}^2+a_{2\alpha}^2\right)\ ,\\
\Gamma_{\alpha\delta} &= \frac{\Gamma_{41}+\Gamma_{42}}{2}(a_{4\alpha}^2+a_{4\delta}^2)+\frac{\Gamma_{21}+\gamma_{22}}{2}(a_{2\alpha}^2+a_{2\delta}^2)\\
&\quad-\gamma_{22}a_{2\alpha}^2a_{2\delta}^2-\Gamma_{42}a_{2\alpha}a_{2\delta}a_{4\alpha}a_{4\delta}+\Lambda_i\left(a_{2\delta}^2+a_{2\alpha}^2-a_{2\alpha}a_{2\delta}a_{4\alpha}a_{4\delta}\right)\ ,\\
\Gamma_{\beta\gamma} &= \frac{\Gamma_{31}+\Gamma_{32}}{2}(a_{3\beta}^2+a_{3\gamma}^2)+\frac{\Gamma_{12}+\gamma_{11}}{2}(a_{1\beta}^2+a_{1\gamma}^2)\\
&\quad-\gamma_{11}a_{1\gamma}^2a_{1\beta}^2-\Gamma_{31}a_{1\beta}a_{1\gamma}a_{3\beta}a_{3\gamma}+\Lambda_i\left(a_{1\gamma}^2+a_{1\beta}^2-a_{1\gamma}a_{1\beta}a_{3\gamma}a_{3\beta}\right)\ ,\\
\Gamma_{\beta\delta} &= \frac{\Gamma_{32}+\Gamma_{31}}{2}a_{3\beta}^2+\frac{\Gamma_{42}+\Gamma_{41}}{2}a_{4\delta}^2+\frac{\Gamma_{21}+\gamma_{22}}{2}a_{2\delta}^2+\frac{\Gamma_{12}+\gamma_{11}}{2}a_{1\beta}^2+\Lambda_i\left(a_{1\beta}^2+a_{2\delta}^2\right)\ ,\\
\Gamma_{\gamma\delta} &= \frac{\Gamma_{32}+\Gamma_{31}}{2}a_{3\gamma}^2+\frac{\Gamma_{42}+\Gamma_{41}}{2}a_{4\delta}^2+\frac{\Gamma_{21}+\gamma_{22}}{2}a_{2\delta}^2+\frac{\Gamma_{12}+\gamma_{11}}{2}a_{1\gamma}^2+\Lambda_i\left(a_{1\gamma}^2+a_{2\delta}^2\right)\ ,
\end{aligned}
\tag{A.3}
$$

The absorption spectrum of a weak probe field along the diagonal channels in the DSP is derived by making use of Eq. (A.1), and the final results read as

$$
\begin{aligned}
A^{dsp}(\omega)\approx\ &+a_{3\beta}^2a_{2\alpha}^2\Gamma_{\beta\alpha}\frac{\langle\sigma_{\alpha\alpha}(\infty)\rangle-\langle\sigma_{\beta\beta}(\infty)\rangle}{\Gamma_{\beta\alpha}^2+\left(\omega-\Omega_{\beta\alpha}\right)^2}+a_{1\beta}^2a_{4\alpha}^2\Gamma_{\beta\alpha}\frac{\langle\sigma_{\beta\beta}(\infty)\rangle-\langle\sigma_{\alpha\alpha}(\infty)\rangle}{\Gamma_{\beta\alpha}^2+\left(\omega+\Omega_{\beta\alpha}\right)^2}\\
&+a_{1\beta}^2a_{4\delta}^2\Gamma_{\beta\delta}\frac{\langle\sigma_{\beta\beta}(\infty)\rangle-\langle\sigma_{\delta\delta}(\infty)\rangle}{\Gamma_{\beta\delta}^2+\left(\omega-\Omega_{\beta\delta}\right)^2}+a_{3\beta}^2a_{2\delta}^2\Gamma_{\beta\delta}\frac{\langle\sigma_{\delta\delta}(\infty)\rangle-\langle\sigma_{\beta\beta}(\infty)\rangle}{\Gamma_{\beta\delta}^2+\left(\omega+\Omega_{\beta\delta}\right)^2}\\
&+a_{3\gamma}^2a_{2\alpha}^2\Gamma_{\gamma\alpha}\frac{\langle\sigma_{\alpha\alpha}(\infty)\rangle-\langle\sigma_{\gamma\gamma}(\infty)\rangle}{\Gamma_{\gamma\alpha}^2+\left(\omega-\Omega_{\gamma\alpha}\right)^2}+a_{1\gamma}^2a_{4\alpha}^2\Gamma_{\gamma\alpha}\frac{\langle\sigma_{\gamma\gamma}(\infty)\rangle-\langle\sigma_{\alpha\alpha}(\infty)\rangle}{\Gamma_{\gamma\alpha}^2+\left(\omega+\Omega_{\gamma\alpha}\right)^2}\\
&+a_{1\gamma}^2a_{4\delta}^2\Gamma_{\gamma\delta}\frac{\langle\sigma_{\gamma\gamma}(\infty)\rangle-\langle\sigma_{\delta\delta}(\infty)\rangle}{\Gamma_{\gamma\delta}^2+\left(\omega-\Omega_{\gamma\delta}\right)^2}+a_{3\gamma}^2a_{2\delta}^2\Gamma_{\gamma\delta}\frac{\langle\sigma_{\delta\delta}(\infty)\rangle-\langle\sigma_{\gamma\gamma}(\infty)\rangle}{\Gamma_{\gamma\delta}^2+\left(\omega+\Omega_{\gamma\delta}\right)^2}
\end{aligned}
\tag{A.4}
$$

## References


[1] Mollow B R 1972 *Phys. Rev. A* **5**(5) 2217–2222 URL https://link.aps.org/doi/10.1103/PhysRevA.5.2217

[2] McCall S L 1974 *Phys. Rev. A* **9**(4) 1515–1523 URL https://link.aps.org/doi/10.1103/PhysRevA.9.1515

[3] Wu F Y, Ezekiel S, Ducloy M and Mollow B R 1977 *Phys. Rev. Lett.* **38**(19) 1077–1080 URL https://link.aps.org/doi/10.1103/PhysRevLett.38.1077
[4] Mompart J and Corbalán R 2000 *J. Opt. B: Quant. Semiclas. Opt.* **2** R7 URL http://stacks.iop.org/1464-4266/2/i=3/a=201
[5] Frogley M D, Dynes J F, Beck M, Faist J and Phillips C C 2006 *Nat. Mater.* **5** 175–178 ISSN 1476-1122 URL http://dx.doi.org/10.1038/nmat1586
[6] Baur M, Filipp S, Bianchetti R, Fink J M, Göppl M, Steffen L, Leek P J, Blais A and Wallraff A 2009 *Phys. Rev. Lett.* **102**(24) 243602 URL https://link.aps.org/doi/10.1103/PhysRevLett.102.243602
[7] Bonadeo N H, Erland J, Gammon D, Park D, Katzer D S and Steel D G 1998 *Science* **282** 14731476 ISSN 0036-8075 URL http://science.sciencemag.org/content/282/5393/1473
[8] Atatüre M, Dreiser J, Badolato A, Högele A, Karrai K and Imamoglu A 2006 *Science* **312** 551–553 ISSN 0036-8075 URL http://science.sciencemag.org/content/312/5773/551
[9] Xu X, Wu Y, Sun B, Huang Q, Cheng J, Steel D G, Bracker A S, Gammon D, Emary C and Sham L J 2007 *Phys. Rev. Lett.* **99**(9) 097401 URL https://link.aps.org/doi/10.1103/PhysRevLett.99.097401
[10] Emary C, Xu X, Steel D G, Saikin S and Sham L J 2007 *Phys. Rev. Lett.* **98**(4) 047401 URL https://link.aps.org/doi/10.1103/PhysRevLett.98.047401
[11] Loo V, Lanco L, Krebs O, Senellart P and Voisin P 2011 *Phys. Rev. B* **83**(3) 033301 URL https://link.aps.org/doi/10.1103/PhysRevB.83.033301
[12] Gerardot B D, Brunner D, Dalgarno P A, Öhberg P, Seidl S, Kroner M, Karrai K, Stoltz N G, Petroff P M and Warburton R J 2008 *Nature (London)* **451** 441–444 ISSN 0028-0836 URL http://dx.doi.org/10.1038/nature06472
[13] Muller A, Flagg E B, Bianucci P, Wang X Y, Deppe D G, Ma W, Zhang J, Salamo G J, Xiao M and Shih C K 2007 *Phys. Rev. Lett.* **99**(18) 187402 URL https://link.aps.org/doi/10.1103/PhysRevLett.99.187402
[14] Kroner M, Weiss K M, Biedermann B, Seidl S, Holleitner A W, Badolato A, Petroff P M, Öhberg P, Warburton R J and Karrai K 2008 *Phys. Rev. B* **78**(7) 075429 URL https://link.aps.org/doi/10.1103/PhysRevB.78.075429
[15] Vamivakas A N, Zhao Y, Lu C Y and Atatüre M 2009 *Nat. Phys.* **5** 198–202 ISSN 1745-2473 URL http://dx.doi.org/10.1038/nphys1182
[16] Flagg E B, Muller A, Robertson J W, Founta S, Deppe D G, Xiao M, Ma W, Salamo G J and Shih C K 2009 *Nat. Phys.* **5** 203–207 ISSN 1745-2473 URL http://dx.doi.org/10.1038/nphys1184
[17] Fernandez G, Volz T, Desbuquois R, Badolato A and Imamoglu A 2009 *Phys. Rev. Lett.* **103**(8) 087406 URL https://link.aps.org/doi/10.1103/PhysRevLett.103.087406
[18] Y ılmaz S T, Fallahi P and Imamoğlu A 2010 *Phys. Rev. Lett.* **105**(3) 033601 URL https://link.aps.org/doi/10.1103/PhysRevLett.105.033601
[19] Fallahi P, Y ılmaz S T and Imamoğlu A 2010 *Phys. Rev. Lett.* **105**(25) 257402 URL https://link.aps.org/doi/10.1103/PhysRevLett.105.257402
[20] Lu C Y, Zhao Y, Vamivakas A N, Matthiesen C, Fält S, Badolato A and Atatüre M 2010 *Phys. Rev. B* **81**(3) 035332 URL https://link.aps.org/doi/10.1103/PhysRevB.81.035332
[21] Li G X, Wu S P and Zhu J P 2010 *J. Opt. Soc. Am. B* **27** 1634–1644 URL http://josab.osa.org/abstract.cfm?URI=josab-27-8-1634
[22] Matthiesen C, Vamivakas A N and Atatüre M 2012 *Phys. Rev. Lett.* **108**(9) 093602 URL https://link.aps.org/doi/10.1103/PhysRevLett.108.093602
[23] Schaibley J R, Burgers A P, McCracken G A, Steel D G, Bracker A S, Gammon D and Sham L J 2013 *Phys. Rev. B* **87**(11) 115311 URL https://link.aps.org/doi/10.1103/PhysRevB.87.115311
[24] Ulhaq A, Weiler S, Roy C, Ulrich S M, Jetter M, Hughes S and Michler P 2013 *Opt. Express* **21** 4382–4395 URL http://www.opticsexpress.org/abstract.cfm?URI=oe-21-4-4382
[25] Ge R C, Weiler S, Ulhaq A, Ulrich S M, Jetter M, Michler P and Hughes S 2013 *Opt. Lett.* **38**

1691–1693 URL http://ol.osa.org/abstract.cfm?URI=ol-38-10-1691

[26] Konthasinghe K, Peiris M, Petrak B, Yu Y, Niu Z C and Muller A 2015 *Opt. Lett.* **40** 1846–1849 URL http://ol.osa.org/abstract.cfm?URI=ol-40-8-1846

[27] Sun Z, Delteil A, Faelt S and Imamoğlu A 2016 *Phys. Rev. B* **93**(24) 241302 URL https://link.aps.org/doi/10.1103/PhysRevB.93.241302

[28] Zajac J M and Erlingsson S I 2016 *Phys. Rev. B* **94**(3) 035432 URL https://link.aps.org/doi/10.1103/PhysRevB.94.035432

[29] Carreño F, Antón M A, Yannopapas V and Paspalakis E 2016 *Phys. Rev. A* **94**(1) 013834 URL https://link.aps.org/doi/10.1103/PhysRevA.94.013834

[30] Carreño F, Maede-Razavi S and Antón M A 2017 *Phys. Rev. B* **95**(19) 195310 URL https://link.aps.org/doi/10.1103/PhysRevB.95.195310

[31] Lagoudakis K G, Fischer K A, Sarmiento T, McMahon P L, Radulaski M, Zhang J L, Kelaita Y, Dory C, Müller K and Vučković J 2017 *Phys. Rev. Lett.* **118**(1) 013602 URL https://link.aps.org/doi/10.1103/PhysRevLett.118.013602

[32] Heinze D, Breddermann D, Zrenner A and Schumacher S 2015 *Nat. Commun.* **6** 8473 URL http://dx.doi.org/10.1038/ncomms9473

[33] Wu Y, Kim E D, Xu X, Cheng J, Steel D G, Bracker A S, Gammon D, Economou S E and Sham L J 2007 *Phys. Rev. Lett.* **99**(9) 097402 URL https://link.aps.org/doi/10.1103/PhysRevLett.99.097402

[34] Ramsay A J, Boyle S J, Kolodka R S, Oliveira J B B, Skiba-Szymanska J, Liu H Y, Hopkinson M, Fox A M and Skolnick M S 2008 *Phys. Rev. Lett.* **100**(19) 197401 URL https://link.aps.org/doi/10.1103/PhysRevLett.100.197401

[35] Press D, Ladd T D, Zhang B and Yamamoto Y 2008 *Nature (London)* **456** 218–221 ISSN 0028-0836 URL http://dx.doi.org/10.1038/nature07530

[36] Press D, Greve K, McMahon P L, Ladd T D, Friess B, Schneider C, Kamp M, Höfling S, Forchel A and Yamamoto Y 2010 *Nat. Photon* **4** 367–370 ISSN 1749-4885 URL http://dx.doi.org/10.1038/nphoton.2010.83

[37] Hildmann J and Burkard G 2014 *Phys. Status Solidi B* **251** 1938–1944 ISSN 1521-3951 URL http://dx.doi.org/10.1002/pssb.201350412

[38] Schulte C H H, Hansom J, Jones A E, Matthiesen C, Le Gall C and Atatüre M 2015 *Nature (London)* **525** 222–225 ISSN 0028-0836 URL http://dx.doi.org/10.1038/nature14868

[39] Xu X, Sun B, Berman P R, Steel D G, Bracker A S, Gammon D and Sham L J 2008 *Nat. Phys.* **4** 692–695 ISSN 1745-2473 URL http://dx.doi.org/10.1038/nphys1054

[40] Brunner D, Gerardot B D, Dalgarno P A, Wüst G, Karrai K, Stoltz N G, Petroff P M and Warburton R J 2009 *Science* **325** 70–72 ISSN 0036-8075 URL http://science.sciencemag.org/content/325/5936/70

[41] Weiss K M, Elzerman J M, Delley Y L, Miguel-Sanchez J and Imamoğlu A 2012 *Phys. Rev. Lett.* **109**(10) 107401 URL https://link.aps.org/doi/10.1103/PhysRevLett.109.107401

[42] Houel J, Prechtel J H, Kuhlmann A V, Brunner D, Kuklewicz C E, Gerardot B D, Stoltz N G, Petroff P M and Warburton R J 2014 *Phys. Rev. Lett.* **112**(10) 107401 URL https://link.aps.org/doi/10.1103/PhysRevLett.112.107401

[43] Kumar P and Nakajima T 2015 *Phys. Rev. A* **91**(2) 023832 URL https://link.aps.org/doi/10.1103/PhysRevA.91.023832

[44] Prechtel J H, Kuhlmann A V, Houel J, Ludwig A, Valentin S R, Wieck A D and Warburton R J 2016 *Nat. Mater.* **15** 981–986 ISSN 1476-1122 URL http://dx.doi.org/10.1038/nmat4704

[45] Antón M A and o F C 2010 *J. Opt.* **12** 104006 URL http://stacks.iop.org/2040-8986/12/i=10/a=104006

[46] Delteil A, Sun Z, Gao W B, Togan E, Faelt S and Imamoglu A 2016 *Nat. Phys.* **12** 218–223 ISSN 1745-2473 URL http://dx.doi.org/10.1038/nphys3605

[47] Xu X, Sun B, Berman P R, Steel D G, Bracker A S, Gammon D and Sham L J 2007 *Science* **317** 929–932 ISSN 0036-8075 URL http://science.sciencemag.org/content/317/5840/929

[48] Xu X, Sun B, Berman P, Steel D G, Gammon D and Sham L 2009 *Solid Stat. Commun.* **149** 1479 – 1484 ISSN 0038-1098 URL http://www.sciencedirect.com/science/article/pii/S0038109809002476

[49] Xu X, Sun B, Kim E D, Smirl K, Berman P R, Steel D G, Bracker A S, Gammon D and Sham L J 2008 *Phys. Rev. Lett.* **101**(22) 227401 URL https://link.aps.org/doi/10.1103/PhysRevLett.101.227401

[50] Warburton R J, Schäflein C, Haft D, Bickel F, Lorke A, Karrai K, García J M, Schoenfeld W and Petroff P M 2000 *Nature* **405** 926–929 ISSN 0028-0836 URL http://dx.doi.org/10.1038/35016030

[51] Ware M E, Stinaff E A, Gammon D, Doty M F, Bracker A S, Gershoni D, Korenev V L, Bădescu c C, Lyanda-Geller Y and Reinecke T L 2005 *Phys. Rev. Lett.* **95**(17) 177403 URL https://link.aps.org/doi/10.1103/PhysRevLett.95.177403

[52] Scully M O and Zubairy M S 1997 *Quantum Optics* (Cambridge: Cambridge University Press) ISBN 0524235953

[53] Lax M 1968 *Phys. Rev.* **172**(2) 350–361 URL https://link.aps.org/doi/10.1103/PhysRev.172.350